The Astrophysical Journal, 686:379–383, 2008 October 10

LOW-TEMPERATURE RATE CONSTANTS FOR ROTATIONAL EXCITATION AND DE-EXCITATION OF C_3 ($X\,^1\Sigma_g^+$) BY COLLISIONS WITH He (^1S)

D. Ben Abdallah,[1] K. Hammami,[1] F. Najar,[1] N. Jaidane,[1] Z. Ben Lakhdar,[1]
M. L. Senent,[2] G. Chambaud,[3] and M. Hochlaf[3]
Received 2007 October 26; accepted 2008 February 18

ABSTRACT

The low-temperature rotational (de-) excitation of C_3 ($X\,^1\Sigma_g^+$) by collisions with He (^1S) is studied using an ab initio potential energy surface (PES). This PES has been calculated using the single- and double-excitation coupled-cluster approach with noniterative perturbational treatment of triple excitations [CCSD(T)] and the augmented correlation-consistent triple-ζ basis set (aug-cc-pVTZ) with bond functions. This PES is then incorporated in full close-coupling quantum scattering calculations for collision energies between 0.1 and 50 cm^{-1} in order to deduce the rate constants for rotational levels of C_3 up to $j = 10$, covering the temperature range 5–15 K.

Subject headings: astrochemistry — infrared: ISM — ISM: molecules — molecular data

Online material: machine-readable table

1. INTRODUCTION

In the near future, the *Herschel* mission will provide a huge amount of highly resolved data in the far-infrared and submillimeter energy domains. The modeling of these highly resolved astrophysical molecular emissions requires the computation of accurate collisional cross sections for these molecules with the abundant H_2 molecule. In previous theoretical determinations of such quantities, He was used rather than H_2 as a collision partner because of its easier theoretical treatment (Ben Abdallah et al. 2003; Lique et al. 2006; Hammami et al. 2007; references therein). Moreover, recent comparative studies have shown that He collisional cross sections are close to those for H_2 and that collisions with He are a reasonable model for collisions with para-H_2, hence validating the use of He rather than H_2 for theoretical treatments and in astrophysical models (Lique et al. 2008). In addition, since C_3 has no permanent dipole moment, the effects of H_2 on collisional cross sections are expected to be equivalent to those obtained with He, further validating the model. This has been shown previously by Phillips (1994) and Faure et al. (2007).

The present work treats the low-temperature nonreactive collisions between He and the C_3 molecular species. In 2000, this carbon cluster was identified in two carbon-rich sources by Cernicharo et al. (2000). These authors observed nine lines of the ν_2 bending mode of triatomic carbon in the direction of Sagittarius B2 and the $R(4)$ and $R(2)$ lines of C_3 in the carbon-rich star IRC +10216. Generally, C_3 and other carbon clusters are expected to be present in several interstellar and circumstellar clouds, and they should be playing a crucial role there during the formation of soot and larger carbon molecules and hydrocarbons (Douglas 1977). C_3 is also seen in diffuse interstellar clouds by virtue of its absorption at visible wavelengths (Roueff et at. 2002; Ádámkovics et al. 2003). The distributions of the levels are used to infer the physical conditions in these clouds. For these reasons, such compounds have attracted major interest in the astrophysical community, and several state-of-the-art laboratory experimental and theoretical investigations have been devoted to the study of their reactivity and spectroscopy (Van Orden & Saykally 1998; Maier 2004; Nicolas et al. 2006; Massó et al. 2006; Senent et al. 2007).

Concerning tricarbon, a large number of investigations have dealt with this astrophysically important molecule, resulting in a huge amount of both theoretical and experimental data. We refer the reader to the review by Van Orden & Saykally (1998) for a detailed discussion of the techniques used for this purpose and for a broad presentation of the results available in the literature for C_3. Briefly, previous spectroscopic studies have established that this carbon cluster is "floppy" in its electronic ground state, with a bending frequency as low as 63 cm^{-1} (Van Orden & Saykally 1998). Theoretical treatments have confirmed this floppy character and shown that the low bending frequency is associated with the flatness of the C_3 ($X\,^1\Sigma_g^+$) potential energy surface (PES) along the bending coordinate. Indeed, a linear, semirigid equilibrium structure has been confirmed at several levels of theory with a flat and broad potential minimum (Van Orden & Saykally 1998). Moreover, it has been shown by Northrup et al. (1991) and Špirko et al. (1997) that the effective bending potential of C_3 ($X\,^1\Sigma_g^+$) spreads up to a bending angle of approximately 40° before reaching the first bending level. Accordingly, in our computations C_3 is considered to be linear, and both C-C distances are set at the experimental r_0-value of 1.2772 Å (Schmuttenmaer et al. 1990).

Here we compute the two-dimensional potential energy surface (2D-PES) of C_3 colliding with He at the coupled-cluster level. The cross sections for the rotational (de-) excitation of C_3 by He at low temperatures (5 K $\leq T \leq$ 15 K) are then deduced using a full close-coupling quantum scattering treatment. The collision energy is deliberately set below the bending anharmonic frequency (i.e., $\leq$63 cm^{-1}) so that only rotational (de-) excitation may occur. How to include rovibrational (de-) excitation is not obvious and needs further theoretical development (D. Ben Abdallah et al. 2008, in preparation). Nevertheless, the present data should be helpful for the identification of this important carbon cluster in the cold interstellar medium. In addition,

[1] Laboratoire de Spectroscopie Atomique-Moléculaire et Applications, Département de Physique, Faculté des Sciences, Université Tunis El Manar, 1060 Tunis Belvédere, Tunisia.
[2] Departamento de Astrofísica Molecular e Infrarroja, Instituto de Estructura de la Materia, CSIC, E-28006 Madrid, Spain; senent@damir.iem.csic.es.
[3] Université Paris-Est, Laboratoire Modélisation et Simulation Multi-Echelle (MSME), FRE 3160 CNRS, F-77454 Marne-la-Vallée Cedex 2, France; hochlaf@univ-mlv.fr.

TABLE 1
CCSD(T) Interaction Energies for C_3-He Obtained with Various Basis Sets for Selected Geometries

θ (deg)	R (B)	Interaction Energy (cm^{-1}) aug-cc-pVTZ	aug-cc-pVTZ + 3*s*3*p*2*d*1*f*	aug-cc-pVQZ	aug-cc-pVQZ + 3*s*3*p*2*d*1*f*
40	4	16280.21	16162.08	16030.80	16005.79
	6.75	207.44	197.22	195.58	191.78
	15	−0.59	−0.59	−0.51	−0.59
90	4	3037.62	2980.98	2968.15	2950.92
	6.75	−22.64	−25.87	−24.41	−26.43
	15	−0.59	−0.38	−0.29	−0.38
CPU time	...	25.33	59.21	226.24	399.24

Note.—These energies are given with respect to the C_3 ($X\,^1\Sigma_g^+$) + He (^1S) asymptote. We also give the CPU time (in minutes) needed for each computation.

the calculations can help in the interpretation of spectra arising from environments that are not in local thermodynamic equilibrium.

2. POTENTIAL ENERGY SURFACE AND ANALYTICAL FIT

The approach of an He (^1S) atom to a C_3 ($X\,^1\Sigma_g^+$) molecule gives rise to one PES, of $^1A'$ symmetry with respect to reflection in the atom-molecule plane. The PES is a function of the three Jacobi coordinates used to describe the C_3-He system: r_0 (the linear C_3 bond distance), R (the distance between the He atom and the center of mass of the C_3 molecule), and θ (the angle between the C_3 axis and R). The interaction energy for each orientation is given by

$$V(R, r_0, \theta) = E_{C_3\text{-He}}(R, r_0, \theta) - E_{C_3}(\infty, r_0) - E_{He}(\infty) + \Delta E_{CP}(R, r_0, \theta),$$

where the counterpoise correction, ΔE_{CP}, is given by

$$\Delta E_{CP}(R, r_0, \theta) = E_{C_3}(\infty, r_0) - E_{C_3}(R, r_0, \theta) + E_{He}(\infty) - E_{He}(R, r_0, \theta).$$

Here $E_{C_3\text{-He}}(R, r_0, \theta)$ is the total energy of the complex at the intermolecular distance R and C_3-He angle θ, and $E_{C_3}(\infty, r_0)$ and $E_{He}(\infty)$ are the energies of the separated fragments. $E_{C_3}(R, r_0, \theta)$ and $E_{He}(R, r_0, \theta)$ are the energies of the fragments calculated with the full basis set for the C_3-He complex. The counterpoise correction compensates for the basis-set superposition error, which arises from lack of saturation of the orbital basis.

The 2D-PES of the C_3-He interacting system was computed using the size-consistent single- and double-excitation coupled-cluster approach, with perturbative treatment of the triple excitations [CCSD(T); Knowles et al. 1993], as implemented in the MOLPRO package (Werner et al. 2002). In preliminary calculations, several basis sets were tested for a proper choice of the most appropriate one, considering the following criteria: (1) a good description of the interaction potential, especially for such weakly bound van der Waals species, and (2) reasonable computing time. These test calculations were performed using Dunning's aug-cc-pVTZ and aug-cc-pVQZ basis sets (Dunning 1989) and additional 3*s*3*p*2*d*1*f* bond basis functions. The results are listed in Table 1 for R-values of 4, 6.75, and 15 B with $\theta = 40°$ and $\theta = 90°$. In all calculations, the bond functions were located in the middle of the van der Waals bond, that is, at $R/2$. As can be seen from this table, the aug-cc-pVTZ + 3*s*3*p*2*d*1*f* and aug-cc-pVQZ + 3*s*3*p*2*d*1*f* basis sets lead to similar results; however, the required CPU time is about 6 times greater for the larger basis set. Similarly, the computed energies using the aug-cc-pVQZ + 3*s*3*p*2*d*1*f* and aug-cc-pVQZ sets are close, but with a factor of 2 increase in CPU time when using the former. Clearly, the addition of basis functions from aug-cc-pVTZ to aug-cc-pVQZ does not affect the quality of the C_3-He PES, especially in the interaction region and the long-range domain, which are important for computations of low kinetic energy collisions between these two species. Accordingly, the present electronic structure calculations were performed using the less expensive aug-cc-pVTZ + 3*s*3*p*2*d*1*f* basis set.

The ab initio potential energies of the C_3 ($X\,^1\Sigma_g^+$) + He (^1S) interacting system were calculated at 10 angles ($\theta = 0°$, $10°$, $20°$, $30°$, $40°$, $50°$, $60°$, $70°$, $80°$, and $90°$) and for 23 values of the scattering coordinate R (ranging from 4 to 25 B). The C_3 molecule is kept at its linear configuration in the electronic ground state of the ground vibrational level as accurately determined by Schmuttenmaer et al. (1990), that is, r_0= 2.414 B (=1.2772 Å). A total of 230 geometries were computed to describe this 2D-PES. The calculated energies were fitted with a least-squares routine to the most convenient analytical form:

$$V(r_0, R, \theta) = \sum_{\lambda=0}^{\lambda_{max}} V_\lambda(r_0, R) P_\lambda(\cos\theta), \quad (1)$$

where P_λ is the Legendre polynomial of order λ and $\lambda_{max} = 18$. It is worth noting that the odd-λ contributions vanish because of the symmetry of the C_3-He potential. The term with $\lambda = 0$ corresponds to the isotropic potential, and the anisotropy of the interacting potential is accounted for by the inclusion of the $\lambda > 0$ terms. The accuracy of the resulting fit was checked by regenerating the potential using equation (1) and comparing directly with the ab initio computed energies for some points outside the grid listed above. The differences were less than 0.5%. In Table 2, the radial dependence of the V_λ-coefficients for $\lambda \leq 18$ is given. Hence, our PES can be generated using these data and equation (1).

Figure 1 displays a two-dimensional contour plot of the C_3-He $X\,^1A'$ electronic ground state correlating to the C_3 ($X\,^1\Sigma_g^+$) + He (^1S) asymptote for fixed C-C distance of r_0 = 2.414 B. The steps between the contours are 3 and 30 cm^{-1} for contours located below and above this asymptote, respectively (see the figure legend for more details). By examining this figure, one can clearly see that the PES presents a shallow potential well in which a T-shaped, weakly bound C_3-He van der Waals complex

TABLE 2

Coefficients $V_\lambda(R)$ of the C_3-He 2D-PES Expansion on the Basis of Legendre Polynomials

R	V_0	V_2	V_4	V_6	V_8	V_{10}	V_{12}	V_{14}	V_{16}	V_{18}
5.0	4395.14	13944.18	11670.94	6695.66	3847.13	2868.82	2871.54	3603.91	6500.25	4597.07
5.25	2946.37	9468.69	7643.99	3848.31	1596.15	657.56	307.29	187.85	210.69	134.76
5.5	1946.84	6379.45	5091.77	2448.21	922.55	320.78	112.22	40.89	18.81	7.77
5.75	1258.51	4216.53	3336.53	1544.99	541.25	168.40	50.90	15.44	5.23	1.65
6.0	796.51	2743.74	2159.56	968.47	318.46	89.81	23.74	5.964	1.29	0.15
6.25	492.68	1760.76	1384.30	604.61	188.24	48.63	11.33	2.35	0.26	−0.07
6.5	296.37	1114.58	879.70	376.21	111.77	26.71	5.52	0.95	0.04	−0.06
6.75	171.69	695.24	554.31	233.31	66.61	14.87	2.77	0.39	−0.01	−0.03
7.0	93.97	426.41	346.23	144.16	39.80	8.37	1.42	0.17	−0.01	−0.02
7.25	46.57	256.15	214.22	88.73	23.86	4.77	0.76	0.09	0.01	−0.00
7.5	18.47	149.71	131.13	54.38	14.32	2.75	0.42	0.05	0.03	0.01
7.75	2.44	84.14	79.26	33.17	8.62	1.60	0.23	0.05	0.03	0.01
8.0	−6.15	44.44	47.16	20.11	5.19	0.95	0.13	0.03	0.01	0.01
8.25	−10.28	20.92	27.47	12.11	3.13	0.34	0.09	0.02	0.01	0.01
8.5	−11.82	7.41	15.54	7.22	1.89	0.21	0.05	0.01	0.01	0.00
8.75	−11.89	−0.02	8.41	4.24	1.14	0.14	0.04	0.01	0.00	0.00
9.0	−11.21	−3.82	4.22	2.45	0.67	0.08	0.02	0.00	0.00	0.00
9.25	−10.18	−5.49	1.83	1.38	0.40	0.06	0.02	0.00	0.00	0.00
9.5	−9.04	−5.96	0.50	0.75	0.23	0.03	0.01	0.00	0.00	0.00
9.75	−7.92	−5.80	−0.18	0.38	0.12	0.01	0.01	0.00	0.00	0.00
10.0	−6.88	−5.32	−0.50	0.17	0.07	0.00	0.00	0.00	0.00	0.00
10.5	−5.12	−4.11	−0.63	0.00	0.00	0.00	0.00	0.00	0.00	0.00
11.0	−3.81	−3.01	−0.52	−0.03	0.00	0.00	0.00	0.00	0.00	0.00
12.0	−2.14	−1.54	−0.26	−0.02	0.00	0.00	0.00	0.00	0.00	0.00
13.0	−1.26	−0.80	−0.11	0.00	0.00	0.00	0.00	0.00	0.00	0.00
14.0	−0.77	−0.44	−0.05	0.00	0.00	0.00	0.00	0.00	0.00	0.00
15.0	−0.49	−0.25	−0.02	0.00	0.00	0.00	0.00	0.00	0.00	0.00

Note.—The V_λ are given in inverse centimeters; R is in bohr units.

can be found. The depth of this potential well is computed to be 25.87 cm^{-1} at the aug-cc-pVTZ + (3*s*3*p*2*d*1*f*)/CCSD(T) level of theory. This value differs by less than 2% if one uses the aug-cc-pVQZ + (3*s*3*p*2*d*1*f*)/CCSD(T) approach (see Table 1). Finally, Figure 1 reveals that the interaction potential depends strongly on the angle of approach of the He atom with respect to the C_3 molecule. Consequently, strong effects of this anisotropy on the rotational transition cross sections are expected, especially at low collision energies of interest here. These findings are in good accord with the relatively large anisotropic terms (V_λ, $\lambda > 0$) given in Table 2 and the cross sections' fluctuations for low kinetic energies (see below).

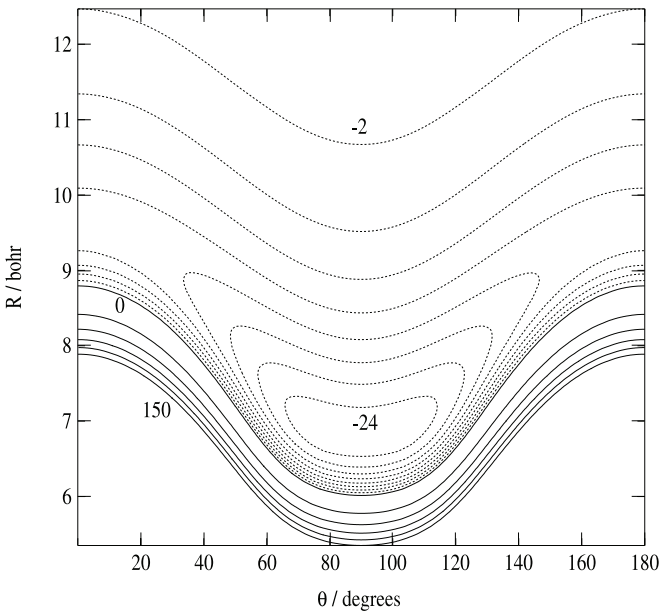

Fig. 1.—Two-dimensional contour plot of the aug-cc-pVTZ + (3*s*3*p*2*d*1*f*)/CCSD(T) PES for the $^1A'$ state correlating to the C_3 ($X\,^1\Sigma_g^+$) + He (^1S) asymptote for fixed C-C distance r_0 = 2.414 B. The highest contour is for 150 cm^{-1}. The spacings are 3 and 30 cm^{-1} between the dotted and solid contours, respectively.

3. SCATTERING CALCULATIONS

The most reliable approach to computing cross sections is to employ the full coupled-cluster method, without further approximations except the use of finite rotational basis sets. In this section, these calculations are performed on our PES, using the hybrid modified logarithmic derivative/Airy propagator of Alexander & Manolopoulos (1987) as implemented in the MOLSCAT quantum mechanical scattering code (Huston & Green 1995).[4] The C_3 molecule is considered to be a rigid rotor. This approximation is valid for the low rotational levels of C_3, located below the bending ν_2 state (at 63 cm^{-1}). Since the experimental rotational constant of C_3 ($X\,^1\Sigma_g^+$) in its ground vibrational state has been evaluated as $B_0 = 0.4305$ cm^{-1} (Schmuttenmaer et al. 1990; Van Orden & Saykally 1998), the present computations allow one to deduce the collisional cross sections up to the $j = 10$ rotational level of C_3.

The scattering computations were carried out using a typical integration R-domain of $R_{min} = 5.0\,B \leq R \leq R_{max} = 25.0\,B$, after some tests with R_{max} ranging from 15.0 to 25.0 B. In order to ensure convergence of the transition cross sections for the six

[4] MOLSCAT is distributed by Collaborative Computational Project No. 6 of the Engineering and Physical Sciences Research Council (UK).

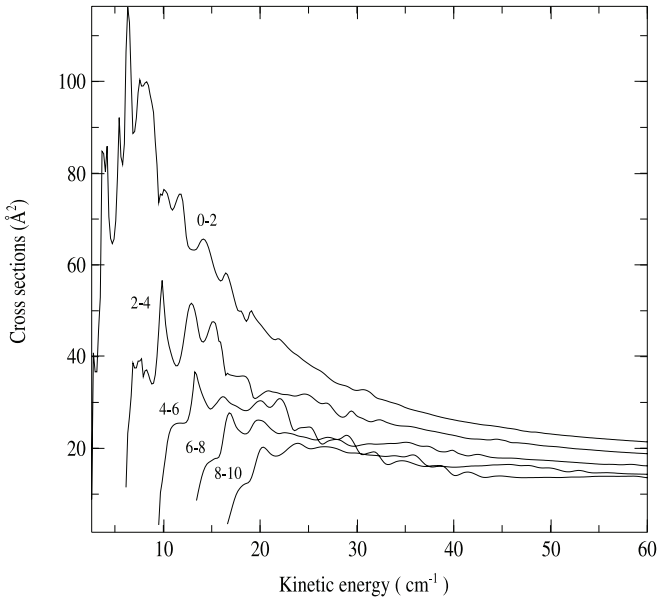

FIG. 2.—Inelastic excitation close-coupling cross sections for C_3 ($X\,^1\Sigma_g^+$) in collision with He (^1S), as a function of kinetic energy.

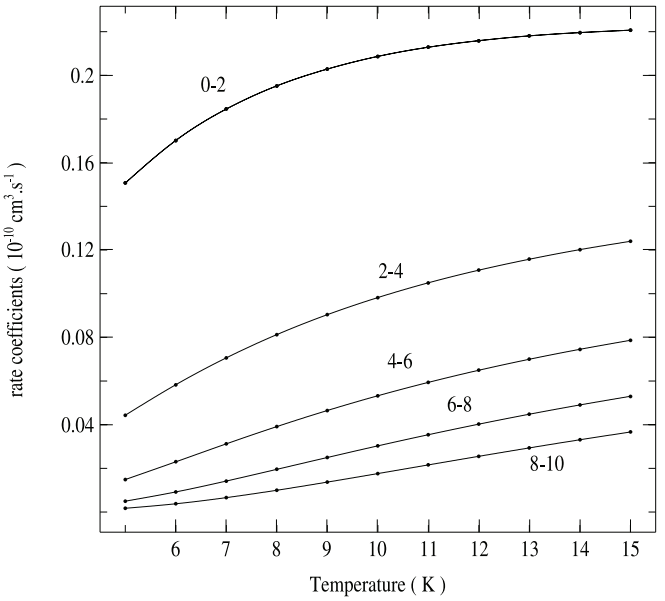

FIG. 3.—Excitation rate coefficients of C_3 ($X\,^1\Sigma_g^+$) in collision with He (^1S), as a function of temperature. (See Table 3.)

lowest C_3 rotational levels (i.e., up to $j = 10$), at least five closed channels were included at each total collision energy (energy collision plus C_3 rotational energy). For the highest transition, $j = 8 \rightarrow j' = 10$, the accuracy is estimated to be about 1.1% and is probably better for lower transitions. The total energies ranged from 0.1 to 180 cm^{-1}. It is worth noting that in these calculations, some energetically inaccessible levels or levels not considered in this work were included in the scattering calculations for a better description of the cross sections. Furthermore, we have also tested the propagation parameters. For instance, the STEPS parameter in MOLSCAT was increased at the lowest energies to constrain the step length of the integrator to below 0.012 B. Moreover, we carefully spanned the energy range to take into account the presence of resonances. The energy steps were 0.1 cm^{-1} below 30 cm^{-1}, 0.5 cm^{-1} from 30 to 50 cm^{-1}, and 1 cm^{-1} from 50 to 180 cm^{-1}. Finally, we emphasize that for the most abundant C_3 isotopomer and because of nuclear spin statistics, the rotational levels with odd values of j are not populated in the C_3 $X\,^1\Sigma_g^+$ state. Therefore, only data for even-j levels are presented in what follows.

Figure 2 displays the variation with kinetic energy of the collisional excitation close-coupling cross sections of C_3 ($X\,^1\Sigma_g^+$) among the six rotational levels with $\Delta j = 2$ (see Table 3 for the excitation rates). Analysis of this figure shows that many resonances can be found for collision energies below 30 cm^{-1}, after which the cross sections present a quite monotonic behavior. Furthermore, the cross sections decrease with increasing j, which is the usual trend for rotational excitation.

The rate coefficients for a given rotational transition can be deduced by averaging the appropriate cross section over a Boltzmann

TABLE 3
EXCITATION AND DE-EXCITATION RATE COEFFICIENTS OF C_3 IN COLLISION WITH He AS A FUNCTION OF TEMPERATURE (5 K < T < 15 K)

j	j'	T (K)	Rate (cm^3 s^{-1})
Excitation Coefficients			
0	0	5.0	0.4440E−09
0	0	6.0	0.4701E−09
0	0	7.0	0.4965E−09
0	0	8.0	0.5232E−09
0	0	9.0	0.5499E−09
De-excitation Coefficients			
2	0	5.0	0.4493E−10
2	0	6.0	0.4485E−10
2	0	7.0	0.4452E−10
2	0	8.0	0.4404E−10
2	0	9.0	0.4350E−10

NOTE.—Table 3 is published in its entirety in the electronic edition of the *Astrophysical Journal*. A portion is shown here for guidance regarding its form and content. See also Figs. 3 and 4.

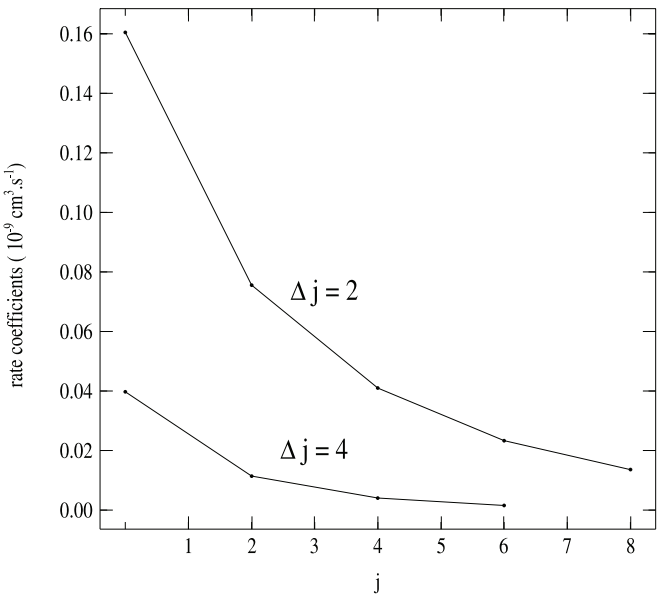

FIG. 4.—Variation of the excitation rate coefficients with initial j-value for different Δj at $T = 10$ K.

distribution of velocities for the incoming atom at a specified temperature T:

$$k_{j\rightarrow j'}(T) = \left(\frac{8}{\pi\mu\beta}\right)^{1/2}\beta^2\int_0^\infty E_k\sigma_{j\rightarrow j'}(E_k)\exp(-\beta E_k)dE_k,$$

where $\sigma_{j\rightarrow j'}$ is the rotational transition cross section, with j and j' being the initial and final rotational quantum numbers, respectively. Here μ is the reduced mass of the system and $\beta = (kT)^{-1}$, and they are related to the reverse transition rate coefficients by

$$k_{j'\rightarrow j}(T) = (2j+1)/(2j'+1)\exp[\beta(E_{j'} - E_j)]k_{j\rightarrow j'}(T).$$

In the expressions above, $E_k = E - E_j$ corresponds to the kinetic energy, where E is the total energy and E_j is the energy of rotational level j.

The full set of computed rate coefficients for rotational levels of C_3 up to $j = 10$ are presented in Table 3. For illustration, Figure 3 depicts the evolution of some $k_{j\rightarrow j'}$ values as a function of temperature for 5 K $\leq T \leq$ 15 K. In Figure 4, we present the rate coefficients' behavior versus initial j-value for different Δj at a kinetic temperature $T = 10$ K. One can clearly see that these rate coefficients decrease sharply with increasing j and Δj and rapidly reach a constant value when T increases. For all transitions, at the lowest temperatures the accuracy of the detailed balance relationship is better than 0.02%.

4. CONCLUSIONS

Using an ab initio potential energy surface for C_3 ($X\,^1\Sigma_g^+$) + He (^1S) followed by a full close-coupling quantum scattering treatment, the collisional rotational (de-) excitations between C_3 X and He have been computed for 5 K $\leq T \leq$ 15 K. These cross sections present several resonances at low kinetic energies KE, and they then decrease with increasing KE, reaching a plateau for KE > 30 cm^{-1}. These data should be useful for the identification of this astrophysically important species in the cold interstellar medium.

The Agencia Española de Cooperación Internacional (project A/8083/07, CSIC–Université Tunis El Manar) and the Spanish Ministerio de Educación y Ciencia (project AYA 2005-00702) are thanked for financial support. M. H. would like to thank the CSIC for a visiting fellowship during the preparation of this work. M. H. and G. C. thank the Physique et Chimie du Milieu Interstellaire program of the Institut National des Sciences de l'Univers (CNRS) for financial support. A. Faure is thanked for a critical reading of the manuscript.

REFERENCES

Ádámkovics, M., Blake, G. A., & McCall, B. J. 2003, ApJ, 595, 235
Alexander, M. H., & Manolopoulos, D. E. 1987, J. Chem. Phys., 86, 2044
Ben Abdallah, D., Jaidane, N., Ben Lakhdar, Z., Spielfiedel, A., & Feautrier, N. 2003, J. Chem. Phys., 118, 2206
Cernicharo, J., Goicoechea, J. R., & Caux, E. 2000, ApJ, 534, L199
Douglas, A. E. 1977, Nature, 269, 130
Dunning, T. H., Jr. 1989, J. Chem. Phys., 90, 1007
Faure, A., Crimier, N., Ceccarelli, C., Valiron, P., Wiesenfeld, L., & Dubernet, M. L. 2007, A&A, 472, 1029
Hammami, K., Lique, F., Jaidane, N., Ben Lakhdar, Z., Spielfiedel, A., & Feautrier, N. 2007, A&A, 462, 789
Hutson, J. M., & Green, S. 1995, MOLSCAT Version 14 User's Manual (New York: Goddard Inst. Space Stud.), http://www.giss.nasa.gov/tools/molscat
Knowles, P. J., Hampel, C., & Werner, H.-J. 1993, J. Chem. Phys., 99, 5219 (erratum 112, 3106 [2000])
Lique, F., Spielfiedel, A., Dhont, G., & Feautrier, N. 2006, A&A, 458, 331
Lique, F., Toboła, R., Kłos, J., Feautrier, N., Spielfiedel, A., Vincent, L. F. M., Chałasiński, G., & Alexander, M. H. 2008, A&A, 478, 567
Maier, J. P. 2004, in The Dense Interstellar Medium in Galaxies, ed. S. Pfalzner et al. (Berlin: Springer), 55
Massó, H., Senent, M. L., Rosmus, P., & Hochlaf, M. 2006, J. Chem. Phys., 124, No. 234304
Nicolas, C., Shu, J., Peterka, D. S., Hochlaf, M., Poisson, L., Leone, S. R., & Ahmed, M. 2006, J. Am. Chem. Soc., 128, 220
Northrup, F. J., Sears, T. J., & Rohlfing, E. A. 1991, J. Mol. Spectrosc., 145, 74
Phillips, T. R. 1994, MNRAS, 271, 827
Roueff, E., Felenbok, P., Black, J. H., & Gry, C. 2002, A&A, 384, 629
Schmuttenmaer, C. A., Cohen, R. C., Pugliano, N., Heath, J. R., Cooksy, A. L., Busarow, K. L., & Saykally, R. J. 1990, Science, 249, 897
Senent, M. L., Massó, H., & Hochlaf, M. 2007, ApJ, 670, 1510
Špirko, V., Mengel, M., & Jensen, P. 1997, J. Mol. Spectrosc., 183, 129
Van Orden, A., & Saykally, R. J. 1998, Chem. Rev., 98, 2313
Werner, H.-J., et al. 2002, MOLPRO: A Package of Ab Initio Programs (ver. 2002.1; Birmingham, UK: Univ. Coll. Cardiff Consultants Ltd.), http://www.molpro.net